

## Multiple-order correlations and convolutions using a spatial light modulator with extended phase range

Ignacio Moreno<sup>a,b,\*</sup>, Jeffrey A. Davis<sup>c</sup>, Benjamin K. Gutierrez<sup>c</sup>, María M. Sánchez-López<sup>a,d</sup>, Don M. Cottrell<sup>c</sup>

<sup>a</sup> Instituto de Bioingeniería, Universidad Miguel Hernández de Elche, 03202 Elche, Spain

<sup>b</sup> Departamento de Ciencia de Materiales, Óptica y Tecnología Electrónica, Universidad Miguel Hernández de Elche, 03202 Elche, Spain

<sup>c</sup> Department of Physics, San Diego State University, San Diego, California 92182-1233, USA

<sup>d</sup> Departamento de Física Aplicada, Universidad Miguel Hernández de Elche, 03202 Elche, Spain

### ARTICLE INFO

#### Keywords:

Optical convolution  
Optical correlation  
Spatial light modulators  
Phase modulation

### ABSTRACT

We present a new type of optical convolver / optical correlator capable of encoding higher orders. The technique is based on obtaining higher powers of a properly designed hologram. This can be obtained in two ways. First, we can recalculate higher orders of the amplitude and phase hologram in a standard spatial light modulator (SLM). More easily, we can utilize a phase-only hologram and exploit the properties of an SLM with extended phase modulation range. Experimental results agree with theory in both cases.

### 1. Introduction

After the pioneering works [1], the use of spatial light modulators (SLM) in optical information processing systems is nowadays generalized [2]. One of the major topics to promote the introduction of SLMs in Optics was optical correlation systems, which was a huge research field by the end of the 20th century when it was considered as a tool for pattern recognition.

Two types of optical architectures were conceived: 1) the 4f system [3,4] and 2) the joint Fourier transform correlator (JFTC) [5,6]. In the 4f system, a two-dimensional input function is optically Fourier transformed and it is multiplied by a second reference function, which is codified in the Fourier transform domain. The convolution or correlation of the two functions is then obtained by a second optical Fourier transform. Both the input function and the Fourier transform of the reference function can be encoded onto SLMs. This correlation architecture presents the great advantage that any desired impulse response can be encoded in the matched Fourier filter, as for instance the phase-only filters that yield optimal light efficiency [7]. However, it imposes strict requirements for the precise alignment of the Fourier filter.

In the JFTC architecture, both the input and reference functions are codified in the space domain with lateral shifts, and the optical Fourier transform gives the joint power spectrum. This intensity pattern is captured by a two-dimensional detector. A second optical Fourier transform of this joint power spectrum provides different terms, one of them being the convolution / correlation of the two patterns. Again, the input and

reference functions, and the joint power spectrum, all can be encoded onto an SLM. The JFTC architecture is advantageous in alleviating alignment requirements. The price paid is a reduction of the space bandwidth product and light efficiency. A further comparison of both approaches was presented in [8].

Despite its long history, this field continues to receive attention [9]. For instance, recent applications include the modal decomposition technique used to identify the modal content of laser beams [10,11], polarization imaging [12] and polarimetric pattern recognition [13], speckle correlation [14] or the development of hybrid optical-electronic convolutional neural networks for image classification [15].

In this work we present a technique for obtaining optical convolutions by displaying higher powers of a properly designed hologram. Given its close relation with convolution, the results are illustrated with the very well-known case of the correlation between two functions. Two ways for obtaining the higher powers of the holograms are presented. First, we recalculate higher orders of the amplitude and phase hologram and use an encoding technique to display the resulting complex functions in a standard spatial light modulator (SLM). This approach provides classical correlation results.

The second approach exploits the properties of an SLM with an extended phase modulation (in this case reaching up to  $10\pi$  phase modulation). In recent works we have been using this extended phase encoding technique in a variety of phase patterns, including diffraction gratings [16,17], diffractive lenses [18] and axicons [19]. Here it is applied to an optical correlator. The technique requires encoding images such that their Fourier transforms are phase-only functions. Then, the different

\* Corresponding author.

E-mail address: [i.moreno@umh.es](mailto:i.moreno@umh.es) (I. Moreno).

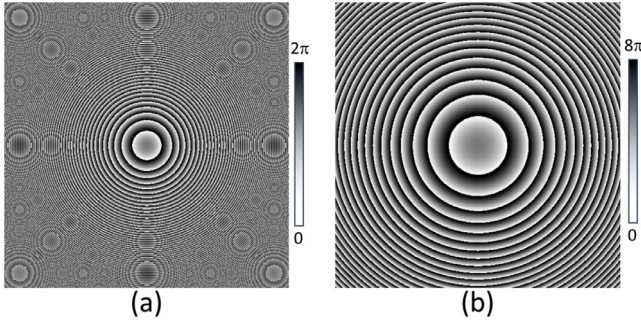


Fig. 1. Lens patterns comparing a focal length of (a) 600 mm and (b) 2400 mm. When the lens in Fig. 1(b) is encoded with  $M = 4$ , it gives the same focus at 600 mm.

powers are obtained by simply displaying the phase-only hologram with different gray-level ranges, resulting in a very simple, fast and effective display method. In addition, it provides the phase-only correlation, thus resulting in very narrow and intense correlation peaks. The second proposed system is similar to that based on the JFTC, but it grants maximum efficiency, since the diffractive mask is a phase-only function.

This process can be extended to obtain higher-order convolutions and correlations. The work by Lohmann and Wirtzner [20] stands as an excellent review as well as giving reasons for their importance, including image processing discussions. Although this field has reduced its activity in recent years, we hope this work inspires further interest.

The paper is organized as follows: First, in Section 2 we discuss the theoretical basis for our approach. In Section 3 we use computer simulations to illustrate the results based on the correlation between two functions. Two experimental setups are discussed in Section 4, one using a standard SLM and the second one using an SLM with extended phase modulation. Section 5 shows the experimental realization of the classical correlation obtained by recalculating different powers of the original Fourier transform hologram and displaying them on the standard SLM. In Section 6 we present the technique that makes the most of the extended phase modulation, and present the corresponding experimental results obtained with the second setup. Finally, Section 7 summarizes the conclusions of our work.

## 2. Optical convolution through high phase modulation

### 2.1. Encoding diffractive elements with SLM exhibiting a large phase range

In general, liquid-crystal SLMs are used to encode a phase-only transmission function  $\exp[i\phi(x, y)]$ , where the phase  $\phi$  takes values in a range of  $2\pi$ . This is typically made by addressing a gray level pattern to the device. However, if the SLM has a large phase modulation range, then the same pattern can be encoded having a maximum phase depth of  $2\pi M$ , where  $M$  is an integer value. In this situation, the function displayed by the SLM acts as if the phase was increased by a factor of  $M$  to become  $\exp[iM\phi(x, y)]$  or, equivalently, as if the  $M$ th-power of the transmission function was displayed.

For example, a blazed diffraction grating having a period  $d$  would normally diffract light into the first order when the phase covers the range from  $0 \leq \phi \leq 2\pi$ . In this case, the transmission of the original function would be  $\exp[i2\pi x/d]$ . However, when the phase range extends over a large modulation range defined by  $M$ , the transmission function would be written as  $\exp[i2\pi Mx/d]$  and the effective period of the grating would act as  $d/M$  [16,17], thus diffracting at larger angles.

Similarly, when a diffractive lens is encoded having a focal length  $f$ , the new transmission function would act as  $\exp[i\pi M r^2/\lambda f]$  and the effective focal length would be  $f/M$ . This situation was exploited to encode lenses that surpass the Nyquist resolution limits imposed by the SLM pixelated structure [18]. As an illustrative example, Fig. 1 shows

this resolution advantage. Fig. 1(a) shows the central  $512 \times 512$  portion of the phase pattern for a lens having a focal length of 600 mm. In the standard case these patterns encode a  $2\pi$  phase shift for gray levels from 0 to 255 (one-byte resolution). Note that this phase pattern is approaching the resolution limits of the device, as inferred from the aliasing effects at the edges. By contrast, Fig. 1(b) shows a lens having a focal length of 2400 mm and the resolution is clearer. In the experiments, this phase pattern is encoded such that gray values of 0 to 255 correspond to phase levels from 0 to  $8\pi$ , i.e.  $M = 4$ . In both cases, the lens forms a focus at 600 mm from the SLM [18]. Although both situations seem in principle equivalent, it is well-known that liquid-crystal on silicon (LCoS) SLMs cannot properly reproduce high spatial frequencies and phase jumps, due to pixel crosstalk generated by the fringing effect [21,22]. Therefore, addressing the image in Fig. 1(b) to the SLM and exploiting high  $M$  values has been proved advantageous in terms of light efficiency [18,19].

Here we further exploit this extended phase modulation regime to generate a new way of optically convolving two functions, when  $M = 2$ , and even obtain higher-order optical convolutions for larger  $M$  values.

### 2.2. Standard convolution – case $M=2$

Let us consider a spatial pattern  $t(\mathbf{x})$  such that its inverse Fourier transform is given by

$$T(\mathbf{p}) = \mathcal{F}^{-1}[t(\mathbf{x})] = \iint_{-\infty}^{+\infty} t(\mathbf{x})e^{+i(\mathbf{p}\cdot\mathbf{x})}d\mathbf{x}d\mathbf{y}, \quad (1)$$

where, for compactness, the functions are written in terms of  $\mathbf{x} = (x, y)$  and  $\mathbf{p} = (p, q) = 2\pi(u, v)$ , where  $(u, v)$  denote the spatial frequencies [4]. In the general situation  $T(\mathbf{p})$  would be a complex-valued function and we assume a technique that allows encoding both its magnitude and its phase information onto a standard SLM device having a maximum phase modulation of  $2\pi$  radians.

We consider the spatial pattern as composed by two functions spatially separated, like in the JFTC system, such that:

$$t(\mathbf{x}) = g(x - a, y) + h(x + a, y). \quad (2)$$

The inverse Fourier transform of this function is written as

$$T(\mathbf{p}) = G(\mathbf{p})e^{+iap} + H(\mathbf{p})e^{-iap}, \quad (3)$$

where  $G(\mathbf{p}) = \mathcal{F}^{-1}[g(\mathbf{x})]$  and  $H(\mathbf{p}) = \mathcal{F}^{-1}[h(\mathbf{x})]$ . If the optical Fourier transform of this function is formed in the focal plane of a lens, the original pattern is recovered.

However, let us consider the case where we encode the function as the square of Eq. (3) and written as

$$[T(\mathbf{p})]^2 = [Ge^{+iap} + He^{-iap}]^2 = G^2e^{+i2ap} + 2GH + H^2e^{-i2ap}. \quad (4)$$

Now the Fourier transform of this function has three terms as

$$t_2(\mathbf{x}) = (g * g) * \delta(x - 2a) + 2(g * h) * \delta(x) + (h * h) * \delta(x + 2a) \quad (5)$$

The first term is the auto-convolution of the first function  $g(\mathbf{x})$  while the third is the auto-convolution of the second function  $h(\mathbf{x})$ . The central term is the convolution  $g * h$  between the two functions. Each of these terms is separated from the others by a distance of  $2a$ , since they are centered at  $x = 0$  and  $x = \pm 2a$ .

### 2.3. Multiple higher-order convolutions - Cases $M=3$ and $M=4$

We continue the discussion for  $M = 3$ . For simplicity, we drop the coordinates in each case. Now the hologram transmission function is modified as

$$[T(\mathbf{p})]^3 = G^3e^{+i3ap} + 3G^2He^{+iap} + 3GH^2e^{-iap} + H^3e^{-i3ap}. \quad (6)$$

and its Fourier transform is given as

$$t_3(\mathbf{x}) = (g * g * g) * \delta(x - 3a) + 3(g * g * h) * \delta(x - a)$$

$$+3(g*h*h)*\delta(x+a) + (h*h*h)*\delta(x+3a). \quad (7)$$

This function has four terms. The first and fourth terms are double auto-convolutions of each of the functions, while the second and third show crossed-convolutions. If the two functions were similar, we would expect the middle two terms to be stronger. Note that their spacing is the same as in Eq. (5), i.e. they are separated by  $2a$ . But they are now centered at spatial locations  $x = \pm a$  and  $\pm 3a$ .

Finally, we form the fourth order representing the case  $M = 4$ . Now, the hologram transmission function is modified as

$$[T(\mathbf{p})]^4 = G^4 e^{+i4ap} + 4G^3 H e^{+i2ap} + 6G^2 H^2 + 4GH^3 e^{-i2ap} + H^4 e^{-i4ap}, \quad (8)$$

and the Fourier transform gives the following output:

$$\begin{aligned} t_4(\mathbf{x}) = & (g * g * g * g) * \delta(x - 4a) \\ & +4(g * g * g * h) * \delta(x - 2a) \\ & +6(g * g * h * h) * \delta(x) \\ & +4(g * h * h * h) * \delta(x + 2a) \\ & +(h * h * h * h) * \delta(x + 4a) \end{aligned} \quad (9)$$

This case shows five output terms, each one involving three convolutions. These terms are now centered at spatial locations  $x = 0$ ,  $x = \pm 2a$  and  $x = \pm 4a$ . In cases where the objects have the same size, we would expect the central term to be the strongest.

Next, we examine numerical simulations for a specific example with correlation effects.

### 3. Numerical simulations using correlation functions

For the rest of this work, we will consider the special case where the function  $h$  is identical to the function  $g$ , except rotated by  $180^\circ$  and complex-conjugated. In this situation, we can use the property so the correlation between two functions is related to their convolution as [4]:

$$g(\mathbf{x}) \oplus h(\mathbf{x}) = g(\mathbf{x}) * h^*(-\mathbf{x}). \quad (10)$$

Thus, by selecting  $t(\mathbf{x})$  in Eq. (2) with  $h(\mathbf{x}) = g^*(-\mathbf{x})$ , we generate a hologram such that

$$\begin{aligned} t(\mathbf{x}) &= g(x-a, y) + g^*(-x-a, -y) \\ \Rightarrow T(\mathbf{p}) &= G(\mathbf{p})e^{iap} + G^*(\mathbf{p})e^{-iap}. \end{aligned} \quad (11)$$

As a consequence, each convolution term  $g * h$  in Eqs. (5), (7) or (9) now becomes an auto-correlation  $g \oplus g$ .

We first consider the case where we can encode both the magnitude and the phase in the holograms. We use a real-valued "L" pattern. Thus, in order to obtain the correlation we simply design  $h$  as the  $(x, y)$  flipped version of  $g$ , as shown in Fig. 2(a). In all the work we use square images of  $1024 \times 1024$  pixels, and Fig. 2(a) shows the central  $640 \times 240$  grid. If we display the Fourier transform hologram  $T(\mathbf{p})$  in Eq. (11) in the standard mode ( $M = 1$ ), we recover this function in Fig. 2(a). In this case, and all those in this section, the hologram's magnitude  $|T(\mathbf{p})|$  is normalized so its maximum value is 1.

However, if the  $M = 2$  case can be realized, Eq. (4) now becomes:

$$[T(\mathbf{p})]^2 = G^2 e^{+i2ap} + 2GG^* + (G^*)^2 e^{-i2ap}. \quad (12)$$

and its Fourier transform is given as:

$$\begin{aligned} t_2(\mathbf{x}) = & (g(\mathbf{x}) * g(\mathbf{x})) * \delta(x - 2a) \\ & +2(g(\mathbf{x}) \oplus g(\mathbf{x})) * \delta(x) \\ & +(g(-\mathbf{x}) * g(-\mathbf{x})) * \delta(x + 2a) \end{aligned} \quad (13)$$

Now the central term is the auto-correlation of  $g(\mathbf{x})$  and is typically quite strong. The two outer terms are auto-convolutions of the upright and inverted letters and they are much weaker.

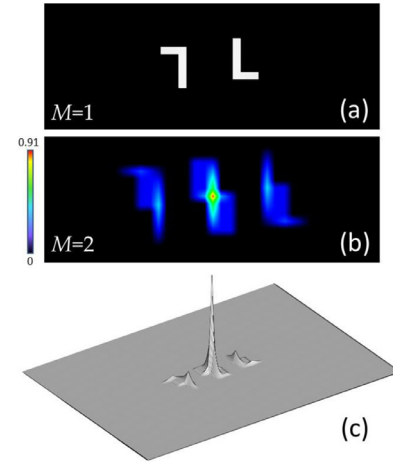


Fig. 2. (a) Input pattern  $t(\mathbf{x}) = g(x-a, y) + g(-x-a, -y)$  consisting of the same symbol "L" where one is inverted and shifted relative to the second. (b) Magnitude of the output  $t_2(\mathbf{x})$  for the Fourier transform of the square ( $M = 2$ ) of the hologram function  $T(\mathbf{p})$ . (c) 3D view of the corresponding intensity.

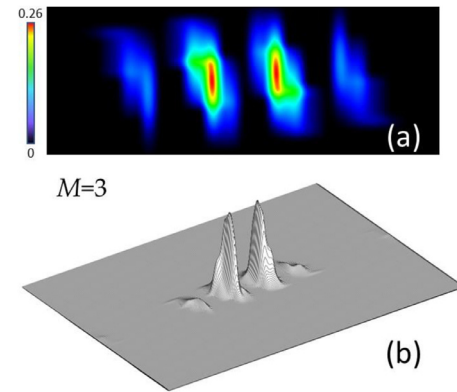


Fig. 3. (a) Magnitude of the output  $t_3(\mathbf{x})$  for the Fourier transform of the cube ( $M = 3$ ) of the hologram function  $T(\mathbf{p})$ . (b) 3D view of the corresponding intensity.

Fig. 2(b) shows the numerical computation of  $t_2(\mathbf{x})$ , where we show its magnitude in order to better see the lateral weaker terms. Its maximum numerical value is  $|t_2|_{\max} = 0.91$ , evaluated relative to the maximum value  $|t_1|_{\max}$  of the "L" reconstruction in Fig. 2(a). Comparison with Fig. 2(a) confirms that the correlation appears centered on axis and lateral auto-convolutions appear centered at  $x = \pm 2a$ , compared to the  $x = \pm a$  locations of the objects in Fig. 2(a). The intensity distribution (magnitude squared) is 3D plotted in Fig. 2(c), showing the three terms in Eq. (13).

If now we choose the case  $M = 3$ , Eq. (6) reads

$$[T(\mathbf{p})]^3 = G^3 e^{+i3ap} + 3G^2 G^* e^{iap} + 3G(G^*)^2 e^{-iap} + (G^*)^3 e^{-i3ap}, \quad (14)$$

and its Fourier transform is then given as

$$\begin{aligned} t_3(\mathbf{x}) = & (g(\mathbf{x}) * g(\mathbf{x}) * g(\mathbf{x})) * \delta(x - 3a) \\ & +3(g(\mathbf{x}) * g(\mathbf{x}) \oplus g(\mathbf{x})) * \delta(x - a) \\ & +3(g(\mathbf{x}) \oplus g(\mathbf{x}) * g(-\mathbf{x})) * \delta(x + a) \\ & +(g(-\mathbf{x}) * g(-\mathbf{x}) * g(-\mathbf{x})) * \delta(x + 3a). \end{aligned} \quad (15)$$

The corresponding simulated results are shown in Fig. 3 which again shows the magnitude of  $t_3(\mathbf{x})$  (Fig. 2(a)) and the 3D representation of the intensity (Fig. 3(b)).

The second and third terms in Eq. (15) provide the auto-correlation convolved with the function itself. In fact, the two letters from Fig. 2(a)

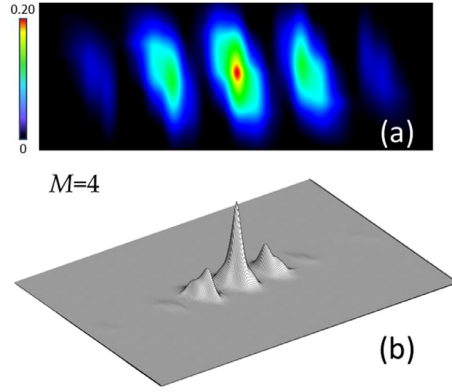


Fig. 4. (a) Magnitude of the output  $t_4(\mathbf{x})$  for the Fourier transform of the cube ( $M = 4$ ) of the hologram function  $T(\mathbf{p})$ . (b) 3D view of the corresponding intensity.

are visible in Fig 3(a), since the convolution with the auto-correlation peak returns the original pattern (assuming that the correlation peak is close to a delta function). A maximum magnitude value  $|t_3|_{\max} = 0.26$  is now obtained, again relative to  $|t_1|_{\max}$ . Note that the spacing between the different terms is the same as in Fig. 2, and these four terms are now centered at  $x = \pm a$  and  $x = \pm 3a$ . The two outer terms are double convolutions of the two functions and are much weaker.

Finally, for the fourth order,  $M = 4$ , Eq. (9) reads

$$[T(\mathbf{p})]^4 = G^4 e^{+i4ap} + 4G^3 G^* e^{+i2ap} + 6G^2 (G^*)^2 + 4G (G^*)^3 e^{-i2ap} + (G^*)^4 e^{-i4ap}, \quad (16)$$

and its Fourier transform is given by the following output

$$t_4(\mathbf{x}) = (g(\mathbf{x}) * g(\mathbf{x}) * g(\mathbf{x}) * g(\mathbf{x})) * \delta(x - 4a) + 4(g(\mathbf{x}) * g(\mathbf{x}) * g(\mathbf{x}) \oplus g(\mathbf{x})) * \delta(x - 2a) + 6(g(\mathbf{x}) \oplus g(\mathbf{x}) * g(\mathbf{x}) \oplus g(\mathbf{x})) * \delta(x) + 4(g(\mathbf{x}) \oplus g(\mathbf{x}) * g(-\mathbf{x}) * g(-\mathbf{x})) * \delta(x + 2a) + (g(-\mathbf{x}) * g(-\mathbf{x}) * g(-\mathbf{x}) * g(-\mathbf{x})) * \delta(x + 4a) \quad (17)$$

Fig. 4 shows the corresponding simulations. The five terms in Eq. (17) are visible in the magnitude of  $t_4(\mathbf{x})$  (Fig. 4(a)). The central term is located on axis and is the strongest. It can be represented as the convolution of the two auto-correlation functions, and therefore adopts the form of a peak, with a maximum value of  $|t_4|_{\max} = 0.20$  relative to  $|t_1|_{\max}$ . However, its width is larger, as shown in Fig. 4, because it is the convolution of the two correlation peaks in Fig. 2(b,c). The rest of the off-axis lateral terms represent different combinations of convolutions and correlations as indicated in Eq. (17), and they are centered at  $x = \pm 2a$  and  $x = \pm 4a$ .

These numerical simulations show the effectiveness of obtaining multiple convolution / correlation terms when displaying  $M$ th-powers of the original Fourier transform hologram. As mentioned before, normally the Fourier transforms involve complex functions with both magnitude and phase information. However, SLMs produce phase-only modulation. In this work we apply two different approaches useful to obtain phase-only holograms that reproduce these higher-order correlations. The first approach is based on encoding the complex valued hologram as a phase-only function and can be displayed onto a standard SLM with  $2\pi$  phase modulation. A second more versatile approach is based on pre-processing the object such that the hologram function  $T(\mathbf{p})$  is already a phase-only function and can then be encoded onto an SLM with extended phase range to obtain the different values of the power  $M$ .

Next, we discuss the two experimental setups employed in this work.

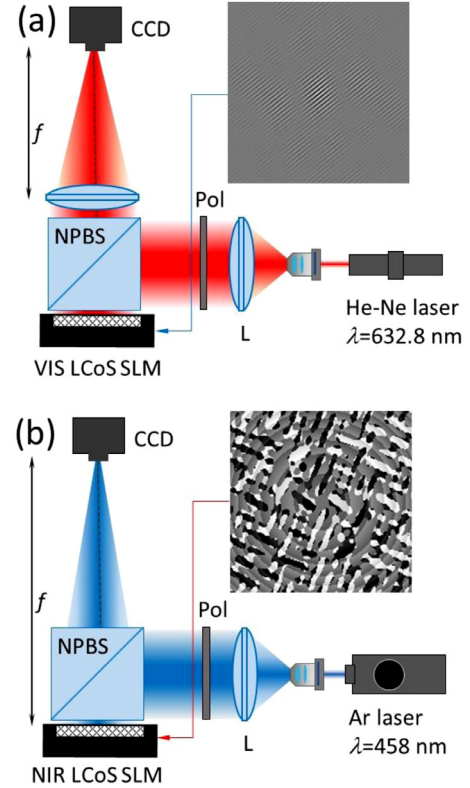


Fig. 5. Scheme of the optical setups. (a) Standard setup with  $2\pi$  phase modulation. (b) Setup with extended phase modulation.

#### 4. Experimental setups

Fig. 5 introduces two similar setups used to experimentally test the former two different approaches. Fig. 5(a) illustrates a standard LCoS-SLM based Fourier transform system. We use an LCoS-SLM device from Hamamatsu (model X10468-01) designed to operate in the visible range. This series of devices have  $792 \times 600$  pixels with a pixel spacing of  $\Delta = 20 \mu\text{m}$ . The device was calibrated between crossed or parallel polarizers and studying the reflection as a function of gray level [24]. In this setup we use the 632.8 nm wavelength of a He-Ne laser, for which the SLM phase modulation is slightly greater than  $2\pi$  radians. The laser beam passes through a spatial filter and a collimating lens and is sent through a non-polarizing beam-splitter (NPBS) to the reflective LCoS-SLM. A linear polarizer selects the polarization component parallel to the liquid-crystal director. The beam is reflected by the SLM and passes again through the NPBS and a lens to the detector, where the Fourier transform of the displayed hologram is reconstructed. The detector is a CCD camera from Basler, model sCA1390-17fc, with  $1390 \times 1038$  square pixels of  $4.65 \mu\text{m}$  side.

A second similar setup is sketched in Fig. 5(b). Here we used the argon ion laser blue line at the shorter wavelength of 458 nm and a Hamamatsu LCoS-SLM (model X10468-08) designed for use in the 1000-1500 nm IR range. Operating this device with this short wavelength provides a large phase modulation depth up to  $10\pi$  [18,19], where  $2\pi$  phase modulation is attained every 50 gray levels. Here we set the phase modulation range up to  $8\pi$  (with gray levels from 0 to 200) to encode phase-only holograms with values  $M = 1, 2, 3, 4$ , where the  $M$  value is controlled by the maximum gray level used to display the hologram. Having 50 phase levels provides a theoretical diffraction efficiency of more than 99.8% [17], and this phase quantization effect can be thus ignored.

The remaining  $2\pi$  phase modulation (provided by the additional gray levels from 201 to 255) is used to encode a diffractive positive lens.

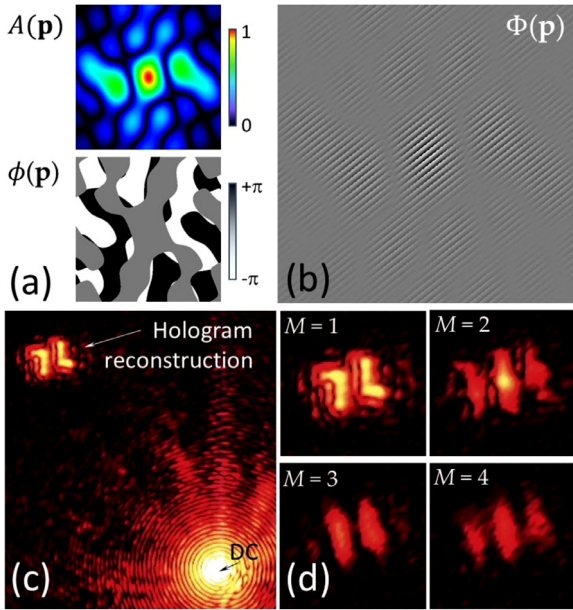


Fig. 6. (a) Magnitude and phase distributions of the hologram function for  $M = 1$ ; (b) the corresponding phase-encoded hologram, (c) wide view of the experimental hologram reconstruction, showing the DC term and the complex hologram reconstruction, and (d) area of the complex hologram reconstruction for cases  $M = 1, 2, 3, 4$ .

We simply add the gray levels of the lens pattern to the gray levels of the hologram pattern to get the combined pattern. We select a lens of focal length 600 mm. This lens produces the optical Fourier transform and its focal plane shows the hologram reconstruction. By encoding the lens function in the SLM (instead of using an external glass lens as in Fig. 4(a)) we reduce the impact of the reflection from the front window of the LCoS device [17]. This reflection comes from the device anti-reflection coating which is designed for IR range and, thus, it is quite strong for the blue light.

## 5. Classical correlation by encoding complex holograms

In the usual case the hologram is a complex function  $T(\mathbf{p}) = A(\mathbf{p})\exp[i\phi(\mathbf{p})]$ . Therefore, in order to reproduce the numerical results in Section 3 we require a technique capable to encode such complex values onto a phase-only function. There are excellent techniques for encoding complex amplitude information onto phase-only devices [25–27]. Here we apply our original method [25] since it has been proven very effective and simple to apply. With this technique, a new phase-only pattern  $\exp[i\Phi(\mathbf{p})]$  is calculated such that the phase distribution to be displayed on the SLM is given by

$$\Phi(\mathbf{p}) = A'(\mathbf{p})[\phi(\mathbf{p}) + \gamma p], \quad (18)$$

where the term  $\gamma p$  corresponds to a blazed grating with a period given by  $1/\gamma$  and the function  $A'(\mathbf{p})$  is calculated to fulfill the condition

$$\frac{\sin[\pi(1 - A'(\mathbf{p}))]}{\pi(1 - A'(\mathbf{p}))} = A(\mathbf{p}), \quad (19)$$

where the magnitude  $A(\mathbf{p})$  is assumed to be normalized to a maximum valued of one. Eq. (19) shows that the maximum phase depth of the blazed grating is spatially modulated with  $A'(\mathbf{p})$ , so the diffraction efficiency in the first diffraction order reproduces this magnitude function  $A(\mathbf{p})$ .

Fig. 6 illustrates the approach. Fig. 6(a) shows the magnitude and the phase distributions for the hologram  $T(\mathbf{p})$  obtained for  $M = 1$ . Only the central area of  $200 \times 200$  pixels of the  $1024 \times 1024$  pixel-array is shown. Fig. 6(b) shows the same  $200 \times 200$  pixels hologram area for the

encoded phase function  $\Phi(\mathbf{p})$  given by Eq. (18), which shows the blazed grating with a phase depth modulated by the magnitude distribution. Note how in the center of the hologram, where the encoded magnitude is maximum, the grating is well reproduced with maximum phase range, while in areas where the magnitude should be low, the grating losses phase depth. This encoded hologram reproduces, in the first diffraction order of the grating, the complex valued hologram.

For this experiment we use the standard setup in Fig. 5(a) since it is not affected by non-desired reflections at the SLM. The corresponding experimental result is shown in Fig. 6(c). A strong DC component appears on axis generated by encoding technique and corresponding to the part of the light is not diffracted. The complex hologram reconstruction (in this case the two “L” patterns) is successfully produced on the direction of the first diffracted order.

Using this approach, we calculated four different phase-encoded holograms, one for each value  $M = 1, 2, 3, 4$ . The area of the hologram reconstruction is shown enlarged in Fig. 6(d) for each case, providing the different correlation terms as described in the numerical results in Section 3. These results agree very well with the numerical simulations in Section 3. In particular, the central auto-correlation peak for  $M = 2$  appears brighter and narrower than for  $M = 4$ . The four images in Fig. 6(d) were captured under the same conditions. As the value of  $M$  increases, the normalized magnitude distribution  $A(\mathbf{p})$  becomes more concentrated in the center. Thus, less intensity is deflected onto the off-axis hologram reconstruction containing the correlation terms, in agreement with the simulated numerical values of Section 3.

Hence, this technique is useful to reproduce the classical correlation results. Nevertheless, a Fourier transform of a pattern like that in Fig. 6(a) presents a very sharp magnitude concentration. Therefore, to produce high-enough diffraction efficiency, the period of the grating in Eq. (18) should extend to at least 8 pixels. Since the width of the central magnitude decreases with  $M$ , it becomes more difficult to fit enough periods of the grating within this central area and the encoding technique becomes less effective. In addition, a different hologram needs to be calculated for each value of the power  $M$ .

Next, we show an alternative and very effective technique that uses a single hologram that is displayed in the LCoS SLM with extended phase modulation to obtain the different powers  $M$ . This technique provides the phase-only correlation, which results in a much narrower correlation peaks, with optimal diffraction efficiency [7].

## 6. Phase-only correlation by displaying a phase-only hologram

Before explaining the phase-only technique, let us remind that the phase-only filter produces an edge-enhancement effect that must be compensated before the technique could be applied.

### 6.1. Encoding with a phase-only filter

Let us illustrate the problem with an object  $g(x)$  consisting again of a letter “L” (Fig. 7(a)). We take the inverse Fourier transform and encode a phase-only hologram where the transmittance is only the phase distribution of  $G(\mathbf{p})$ . Now when we take the Fourier transform of this hologram to recover the original object, an edge-enhancement effect is produced, mostly visible in the corners of the “L” pattern (Fig. 7(b)). This occurs because the loss of the magnitude information in the Fourier domain enhances the relative weight of the high spatial frequency components [7]. Restoring the information lost due to the hologram phase-only encoding is an important topic in computer-generated holography. This also affects our technique. Therefore, it is necessary to compensate for this effect.

One option consists in adding a random phase pattern to the original object and applying iterative algorithms [28]. Here instead we use a previously discussed simple approach [29] where we multiply the original image by a binary (1,0) random pattern as shown in Fig. 7(c). Again, we

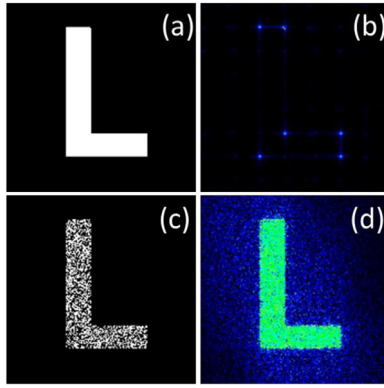


Fig. 7. (a) Original object. (b) Magnitude of the output for a phase-only hologram of (a). (c) Original object multiplied by random binary pattern (d) Magnitude of the output for a phase-only hologram of (c).

take the inverse Fourier transform and consider only the phase distribution. Now, because the original object is filled with high-frequency content, the edge-enhanced version returns a good representation of the original object as shown in Fig. 7(d). Additional random noise is expected around the object reconstruction, as shown in the Fig.. This way, it is not necessary to apply complex-valued encoding techniques or iterative techniques.

## 6.2. Results for the phase-only correlation

In this situation where new functions with added random noise, like in Fig. 7(c), are used to calculate the phase-only holograms, we expect much sharper correlation functions. This is the case of the phase-only matched filter [7] compared to the classical correlation filter. The corresponding numerical simulation is shown in Fig. 8, which reproduces numerical calculations of the hologram reconstructions  $t_1(\mathbf{x})$ ,  $t_2(\mathbf{x})$ ,  $t_3(\mathbf{x})$  and  $t_4(\mathbf{x})$  now calculated using the “L” pattern with added random pattern and considering the phase-only version of the hologram.

Fig. 8(a) shows the central area of the phase-only hologram. As opposed to the previous Section, it does not require adding a carrier linear phase to operate off-axis. Therefore, the phase pattern does not exhibit the high frequency content shown in Fig. 6(b). The other images in Fig. 8 display the intensity distributions of the Fourier transform output for the different cases. The case  $M = 1$  (Fig. 8(b)) shows the direct and inverted “L” patterns, which appear filled (no edge enhancement) with the expected additional noise.

The case  $M = 2$  (Fig. 8(c1)) shows a very narrow and intense correlation peak that appears on axis, corresponding to the central  $g \oplus g$  term in Eq. (12). To better visualize this correlation peak, the intensity pattern in Fig. 8(c1) was truncated to 1% of the maximum value. In addition, Fig. 8(c2) shows a 3D view of the magnitude distribution of the correlation peak. Here we magnified the image by a factor of about 5 and we show only the central area of  $128 \times 128$  pixels of the output plane.

Because the correlation peak in Fig. 8(c2) is almost a perfect delta function, the additional convolution term obtained for  $M = 3$  yields the arising of the two “L” patterns again for this case (Fig. 8(d)). Finally, for  $M = 4$ , Fig. 8(e1) we obtain again an on-axis a peak corresponding to the term  $(g \oplus g * g \oplus g)$  in Eq. (16) i.e., the convolution of the auto-correlations. Fig. 8(e2) shows the 3D plot, again only showing a  $128 \times 128$  portion of the magnitude distribution, which shows no difference compared with the  $M = 2$  case.

Fig. 9 shows the corresponding experimental results that reproduce these previous numerical simulations. They have been obtained in the setup in Fig. 5(b). We highlight that only a single hologram is calculated (as shown in Fig. 8(a)) and we use the large phase modulation of the

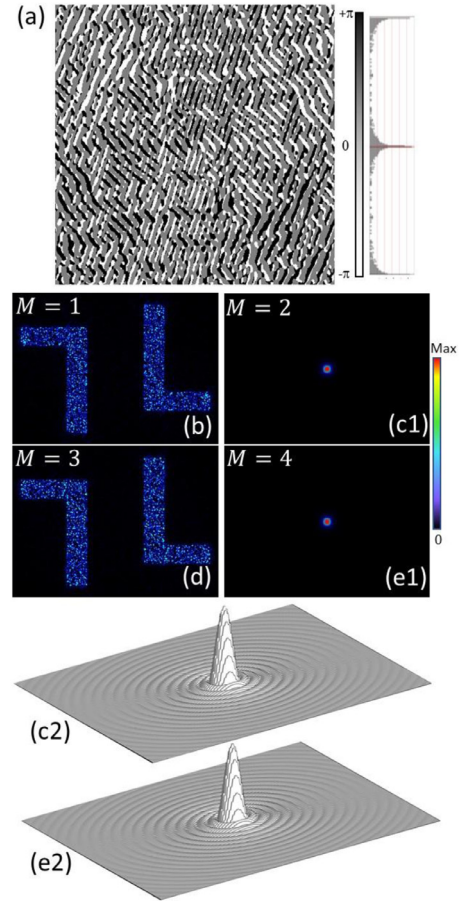


Fig. 8. (a) Phase-only hologram obtained for a “L” pattern encoded with random noise. Its corresponding intensity output at the Fourier transform plane for: (b)  $M = 1$ , (c1)  $M = 2$ , (d)  $M = 3$ , and (e1)  $M = 4$ . Images in (c1) and (e1) have been truncated to 1% of the maximum value to better view the correlation peak. (c2) and (e2) show the 3D representation of the magnitude distribution of the correlation peak.

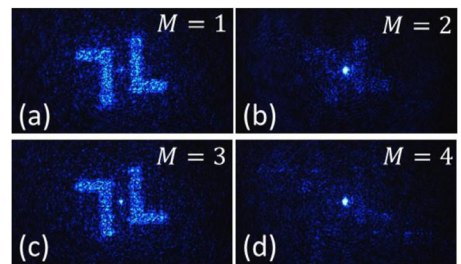


Fig. 9. Experimental correlation results obtained after Fourier transforming the phase-only hologram with different phase-modulation ranges: (a)  $M = 1$ , (b)  $M = 2$ , (c)  $M = 3$  and (d)  $M = 4$ . Cases (b) and (d) show the correlation peaks.

device in this setup to achieve the different powers  $M$ . For each case, the hologram is displayed on the SLM with different phase modulation depths. This is obtained applying a gray level range that changes from 0-50, 0-100, 0-150, and 0-200 for  $M = 1, 2, 3, 4$ , respectively.

These experimental results agree very well with the numerical simulations presented in Fig. 8. For  $M = 1$  (Fig. 9(a)) we obtain the standard hologram response where the two “L” patterns appear spatially separated and inverted, with some noise generated by the added random pattern, but the edge-enhancement effect is successfully eliminated.

The result for  $M = 2$  (Fig. 9(b)) shows the auto-correlation clearly visible in the form of a bright narrow peak of light that appears on axis. For  $M = 3$  (Fig. 9(c)), we obtain again the two “L” patterns, in agreement with the previous discussion of Fig. 8(c). And finally, for  $M = 4$  (Fig. 9(d)) we obtain again a very narrow and intense correlation peak.

## 7. Conclusions

In summary, this work examines the capability to perform higher-order convolutions and correlations by encoding powers of a Fourier transform hologram. Two different approaches are considered, both showing excellent agreement between numerical calculations and experiments.

First, we can formulate the desired original complex amplitude hologram and calculate its powers digitally. The resulting hologram is displayed onto a phase-only SLM using a technique to encode complex values [25]. The desired order is achieved by taking the Fourier transform of the encoded pattern. This approach is able to reproduce the classical correlation and it is demonstrated with a standard SLM of  $2\pi$  phase modulation.

Second, we illustrate how the multiple powers of the hologram transmission can be realized using a phase-only SLM of extended phase modulation range  $M2\pi$ , provided the Fourier transform hologram is a phase-only function. Proof of this is provided using holograms designed for a binary object with added random pattern. In this case, the desired order is obtained on axis since the technique does not require adding a linear phase. Therefore, the approach is less likely to be affected by the fringing effect [21], that might reduce the diffraction efficiency of high frequency patterns [19,22]. With this second approach the different powers of the hologram are achieved by simply changing the phase depth of the displayed gray level mask. Furthermore, it provides a phase-only correlation.

This second approach combines some of the advantages of the 4f and the JFTC correlator systems. It provides a phase-only correlation, which is attractive in terms of diffraction efficiency and correlation sharpness. This property was typically obtained in the 4f correlator configuration when SLMs were used to display phase-only filters. However, the 4f system requires a very precise alignment of the displayed Fourier filter. On the other side, our approach resembles the JFTC system since the two correlated functions must be displayed with a lateral shift in order to calculate the hologram in the Fourier domain. This hologram is optically Fourier transformed to provide the correlation function. This approach alleviates the alignment requirements, as in the JFTC system.

Research activity in optical correlation and convolution has notably diminished in comparison with that in the nineties. This novel and simple way to obtain higher-order correlations and convolutions might lead to renovated interest. The work by Lohmann and Wirmitzer [20] provides ample reasons for further investigations. Approaches like modal decomposition [10,11], polarimetric pattern recognition [12], polarization imaging [13], speckle correlation [14], convolutional neural networks [15] or others as reviewed in [9] might benefit from it.

## Declaration of Competing Interest

The authors declare that they have no known competing financial interests or personal relationships that could have appeared to influence the work reported in this paper.

## CRediT authorship contribution statement

**Ignacio Moreno:** Conceptualization, Methodology, Investigation, Formal analysis, Writing – review & editing. **Jeffrey A. Davis:** Conceptualization, Methodology, Investigation, Formal analysis, Writing – review & editing. **Benjamin K. Gutierrez:** Methodology, Investigation.

**María M. Sánchez-López:** Methodology, Investigation, Writing – review & editing. **Don M. Cottrell:** Software, Formal analysis.

## Acknowledgements

Ignacio Moreno and María M. Sánchez-López acknowledge funding from Conselleria d'Educació, Investigació, Cultura i Esport; Generalitat Valenciana (PROMETEO-2017-154); and Ministerio de Ciencia, Innovación y Universidades (Ministerio de Ciencia e Innovación (MICINN) (RTI2018-097107-B-C33).

## References

- [1] Liu HK, Davis JA, Lilly RA. Optical-data-processing properties of a liquid-crystal television spatial light modulator. *Opt Lett* 1985;10(12):635–7.
- [2] Haist T, Osten W. Holography using pixelated spatial light modulators - part 1: theory and basic considerations. *J Micro/Nanolithogr MEMS MOEMS* 2015;14(4):041310.
- [3] Vander Lugt A. Signal detection by complex spatial filtering. *IEEE Trans Inform Theory* 1964;IT-10(2):139–45.
- [4] Goodman JW. *Introduction to Fourier Optics*. McGraw Hill; 1969.
- [5] Weaver CS, Goodman JW. Technique for optically convolving two functions. *Appl Opt* 1966;5(7):1248–9.
- [6] Yu FTS, Ludman JE. Microcomputer-based programmable optical correlator for automatic pattern recognition and identification. *Opt Lett* 1986;11(6):395–7.
- [7] Horner JL, Gianino PD. Phase-only matched filtering. *Appl Opt* 1984;23(6):812–16.
- [8] Lu XJ, Yu FTS, Gregory DA. Comparison of Vander Lugt and joint transform correlators. *Appl Phys B* 1990;51:153–64.
- [9] Millán MS. Advanced optical correlation and digital methods for pattern matching—50<sup>th</sup> anniversary of Vander Lugt matched filter. *J Opt* 2012;103001.
- [10] Flamm D, Naidoo D, Schulze C, Forbes A, Duparré M. Mode analysis with a spatial light modulator as a correlation filter. *Opt Lett* 2012;37(13):2478–80.
- [11] Pachava S, Dixit A, Srinivasan B. Modal decomposition of Laguerre Gaussian beams with different radial orders using optical correlation technique. *Opt Express* 2019;27(9):13182–93.
- [12] Carnicer A, Arteaga O, Pascual E, Canillas A, Vallmitjana S, Javidi B, Bertran E. Optical security verification by synthesizing films with unique polarimetric signatures. *Opt Lett* 2015;40(22):5399–402.
- [13] Han P, Liu F, Wei Y, Shao X. Optical correlation assists to enhance underwater polarization imaging performance. *Opt Lasers Eng* 2020;134:106256.
- [14] Vijayakumar A, Jayavel D, Muthaiah M, Bhattacharya S, Rosen J. Implementation of a speckle-correlation-based optical lever with extended dynamic range. *Appl Opt* 2019;58(22):5982–8.
- [15] Chang J, Sitzmann V, Dun X, Heidrich W, Wetzstein G. Hybrid optical-electronic convolutional neural networks with optimized diffractive optics for image classification. *Sci Rep* 2018;8:12324.
- [16] Albero J, García-Martínez P, Martínez JL, Moreno I. Second order diffractive optical elements in a spatial light modulator with large phase dynamic range. *Opt Lasers Eng* 2013;51:111–15.
- [17] Moreno I, Gutierrez BK, Sánchez-López MM, Davis JA, Khanal HP, Cottrell DM. Diffraction efficiency of stepped gratings using high phase-modulation spatial light modulators. *Opt Lasers Eng* 2020;126:105910.
- [18] Gutierrez BK, Davis JA, Moreno I, Cottrell DM. Encoding lenses with focal lengths lower than the Nyquist limit using high phase-modulation displays. *Opt Lett* 2019;44(13):3398–401.
- [19] Gutierrez BK, Davis JA, Sánchez-López MM, Moreno I, Cottrell DM. Dynamic control of Bessel beams through high-phase diffractive axicon. *OSA Continuum* 2020;3(5):1314–21.
- [20] Lohmann AW, Wirmitzer B. Triple correlations. *Proc IEEE* 1984;72:889–901.
- [21] Efron U, Apter B, Bahat-Treidel E. Fringing-field effect in liquid-crystal beam-steering devices: an approximate analytical model. *J Opt Soc Am A* 2004;21(10):1996–2008.
- [22] Davis JA, Wolfe ED, Moreno I, Cottrell DM. Encoding complex amplitude information onto phase-only diffractive optical elements using binary phase Nyquist gratings. *OSA Continuum* 2021;4(3):896–910.
- [24] Davis JA, Tsai P, Cottrell DM, Sonehara T, Amako J. Transmission variations in liquid crystal spatial light modulators caused by interference and diffraction effects. *Appl Opt* 1999;38(6):1051–7.
- [25] Davis JA, Cottrell DM, Campos J, Yzuel MJ, Moreno I. Encoding amplitude information onto phase-only filters. *Appl Opt* 1999;38(23):5004–13.
- [26] Arrizón V. Optimum on-axis computer-generated hologram encoded into low-resolution phase-modulation devices. *Opt Lett* 2003;28(24):2521–3.
- [27] Clark TW, Offer RF, Franke-Arnold S, Arnold AS, Radwell N. Comparison of beam generation techniques using a phase only spatial light modulator. *Opt Express* 2016;24(6):6249–64.
- [28] Wyrowski F. Diffractive optical elements: iterative calculation of quantized, blazed phase structures. *J Opt Soc Am A* 1990;7(6):961–9.
- [29] Davis JA, Flowers SW, Cottrell DM, Lilly RA. Smoothing of the edge-enhanced impulse response from binary phase-only filters using random binary patterns. *Appl Opt* 1989;28(15):2987–8.